



ANALYTICAL AND NUMERICAL STUDY ON FREE VERTICAL VIBRATION OF SHEAR-FLEXIBLE SUSPENSION BRIDGES

M.-Y. KIM

*Department of Civil Engineering, Sung Kyun Kwan University, Jangan-Gu, Suwon, Kyongki-Do,
440-746, South Korea. E-mail: kmye@yurim.skku.ac.kr*

S.-D. KWON

*Department of Civil & Environmental Engineering, Dongyang University, Youngju, Kyongbuk, 750-711,
South Korea*

AND

N.-I. KIM

*Department of Civil Engineering, Sung Kyun Kwan University, Jangan-Gu, Suwon, Kyongki-Do,
440-746, South Korea*

(Received 2 September 1998, and in final form 12 May 2000)

This study develops an analytical and numerical method for free vertical vibration of suspension bridges including shear deformation and rotary inertia. Under the assumption that the vertical displacement of the main cable is identical to that of the stiffening girder, the differential equation of motion containing three new terms are derived based on Timoshenko's beam-column theory. The general analytical method for determining natural frequencies and mode shapes of hinged- and continuous-suspension bridges are presented. Special consideration is given to evaluating the natural frequency of simply supported three-span suspension bridges. For finite element analysis, the suspension bridge element is developed by using Hermitian polynomials considering shear effects. The full truss model, in which both cable and truss girder is modelled by a truss element, is used in order to investigate the accuracy of the presented suspension bridge theory. Numerical examples are provided to illustrate the applicability and effectiveness of the present analytical and numerical method.

© 2000 Academic Press

1. INTRODUCTION

The suspension bridge is recognized as the most suitable bridge type for the long-span scenarios and as such all of the bridges that exceed 1000 m span length are suspension bridges. However, the flexibility caused by the cable system and its long span makes the suspension bridge sensitive to dynamic loads. In order to approach dynamic problem such as wind, vehicle or earthquake-induced oscillation, it is necessary to develop a simple method of determining accurate natural frequencies and mode shapes.

Early attempts on free vibration of suspension bridge were made by Moisseiff who extended the elastic theory to the deflection theory. Steinman [1] and Bleich *et al.* [2] derived some formulas for computing natural frequencies and mode shapes based on the so

called linearized deflection theory. However, some factors like shear deformation and rotary inertia, and so forth were neglected for simplicity. In the late 1970's Abdel-Ghaffar [3–5] developed the methodology of free vertical, torsional and lateral vibration analysis of suspension bridges by means of a variational principle and a finite element approach that neglected shear deformation effects. Hayashikawa [6] derived the method of free vertical vibration based on linearized deflection theory considering shear deformation and rotary inertia. Hayashikawa [7] also took into account the effect of gravitational stiffness due to dead loads on the stiffening girder for free torsional vibration. But he did not address the occurrence of double-root frequencies at higher symmetric and anti-symmetric mode shapes of hinged three-span suspension bridges.

Even though the effect of shear deformation and rotary inertia are relatively small in comparison with that of bending deformation, it should be pointed out that the effect of shear deformation can be increased when the stiffening truss is replaced with an equivalent beam for analysis. Timoshenko and Gere [8], Chugh [9], Kim [10] and many investigators have studied the effect of shear deformation on the beam.

This study intends to develop an analytical and numerical method for free vertical vibration of suspension bridges including shear deformation and rotary inertia. By applying Hamilton's Principle, the differential equation of motion and boundary condition are derived from the kinetic and potential energy of the cable and stiffening girder. A general analytical procedure for finding natural frequencies and mode shapes of simply supported suspension bridge considering the effects of shear deformation and rotary inertia is presented based on the exact solution of the fourth order differential equation of motion. In using this method, three new terms are included for comparison with previous studies [3, 6]. Both symmetric and anti-symmetric mode with the same natural frequency without tension increment are observed in the hinged three-span suspension bridge.

For evaluating natural frequencies of continuous suspension bridge, Hayashikawa's method [6] is applied. For finite element analysis, the shear flexible suspension bridge element is developed by using the Hermitian polynomials that take into consideration the shear deformation effects. The full truss model, in which the main cable, hanger, and truss girder are modelled by the truss element, respectively, is presented for comparison. Finally, detailed numerical examples are provided to illustrate the applicability and effectiveness of the present method and rigorous comparison is made with the analytical solutions, numerical results from the suspension bridge element and the full truss model.

2. BASIC ASSUMPTIONS

The following general assumptions and approximations are made.

- (1) All materials in the bridge follow Hooke's law. Hangers are inextensible. Flexural stiffness of the cable is negligible.
- (2) The initial dead load is carried by the main cable without causing stress in the stiffening girder.
- (3) The cable is assumed to be of uniform cross-section and of a parabolic profile under dead load.
- (4) Vertical vibration of the cable is identical to that of the stiffening girder.
- (5) The additional horizontal component of cable tension $H(t)$ caused by vibration is identical throughout each span and is small in comparison with the initial horizontal component of cable tension H_w .

3. DIFFERENTIAL EQUATION OF MOTION

In order to take into account the effect of shear deformation and rotary inertia, Timoshenko's beam-column theory is applied in this study instead of the Bernoulli–Euler beam theory. The differential equation of motion of a suspension bridge and their associated boundary conditions are derived by means of Hamilton's principle and are given as follow:

$$\delta \int_{t_1}^{t_2} (T - V) dt = 0, \quad (1)$$

where T and V are kinetic and potential energy of the suspension bridge respectively. The kinetic and potential energy of the bridge considering rotary inertia and shear deformation can be written as

$$T = \frac{1}{2} \sum_{i=1}^3 \int_0^{l_i} (m_i \dot{v}_i^2 + \rho_{gi} I_{gi} \dot{\beta}_i^2) dx_i \quad (2a)$$

$$V = \frac{1}{2} \sum_{i=1}^3 \int_0^{l_i} \left[E_{gi} I_{gi} \beta_i'^2 + \frac{G_i A_{gi}}{f_{si}} (v_i' - \beta_i)^2 + H_w v_i'^2 \right] dx_i + \frac{1}{2} \frac{H^2(t) L_E}{E_c A_c}, \quad (2b)$$

in which v_i is the translational displacement, β_i the rotational displacement, m_i the mass of the bridge per unit length, ρ_i the mass density, E the modulus of elasticity, G the shear modulus, A_g the cross sectional area, I_g the moment of inertia, and f_s the shear coefficient. Suffix i represents the i th span of the bridge, suffix g and c denote stiffening girder and cable respectively. The notation $(\dot{\cdot})$ and (\prime) represent partial derivative of time, t and space, x respectively. Virtual length of the cable L_E is defined by

$$L_E = \sum_{i=1}^3 L_{ei} = \sum_{i=1}^3 l_i \left[1 + 8 \left(\frac{f_i}{l_i} \right)^2 \right]. \quad (3)$$

When the stiffening truss girder is modelled as an equivalent Timoshenko beam, A_g is the sum of the cross-sectional area of top and bottom chords, I_g is the area moment of inertia of top and bottom chords about its neutral axis, and f_s is the shear coefficient.

The shear coefficient is dependent on the shape of stiffening girder and its detailed formulas for typical truss girders are summarized in Table 1. Timoshenko and Gere [8] presented the relation between the lateral displacement and shear force of a laced column. This relation can be used to derive the shear coefficient of truss girder. Some of the shear coefficients in Table 1 can be found in reference [4], and the other shear coefficients are derived based on the theory presented by Timoshenko and Gere.

The additional horizontal component of cable tension $H(t)$ can be expressed as

$$H(t) = \frac{E_c A_c}{L_E} \sum_{i=1}^3 [u_i(l_i) - u_i(0)] + \frac{E_c A_c}{L_E} \sum_{i=1}^3 \frac{m_i g}{H_w} \int_0^{l_i} v_i dx_i, \quad (4)$$

where u_i is the longitudinal displacement in the i th span. Substituting equation (2) into equation (1) and applying Hamilton's principle, the following differential equations of

TABLE 1
Shear coefficient of various truss types

Truss	Shape	Shear coefficient
1	N-type	$f_s = \frac{AG}{E} \left[\frac{A_v + A_d \sin^3 \phi}{A_d A_v \sin^2 \phi \cos \phi} \right]$
2	Modified warren	$f_s = \frac{AG}{A_d E \sin^2 \phi \cos \phi}$
3	Warren	$f_s = \frac{AG}{A_d E \sin^2 \phi \cos \phi}$
4	Multi-web	$f_s = \frac{AG}{2A_d E \sin^2 \phi \cos \phi}$
5	Double warren	$f_s = \frac{AG}{2A_d E \sin^2 \phi \cos \phi}$
6	K-type	$f_s = \frac{AG}{E} \left[\frac{A_v + A_d \sin^3 \phi}{2A_d A_v \sin^2 \phi \cos \phi} \right]$

Note: A_d is the cross-sectional area of diagonal member; A_v the cross-sectional area of vertical member; and A the cross-sectional area of top and bottom chord.

motion are obtained:

$$m_i \ddot{v}_i - H_w v_i'' + \frac{m_i g}{H_w} H(t) - \frac{G_i A_{gi}}{f_{si}} (v_i'' - \beta_i'') = 0, \tag{5a}$$

$$\rho_{gi} I_{gi} \ddot{\beta}_i - E_{gi} I_{gi} \beta_i'' - \frac{G_i A_{gi}}{f_{si}} (v_i' - \beta_i') = 0. \tag{5b}$$

In the same manner, boundary conditions at the end of each span ($x_i = 0, l_i$) are also found to be as follows:

$$E_{gi} I_{gi} \beta_i' = 0 \quad \text{or} \quad \delta \beta_i = 0, \tag{6a}$$

$$H_w v_i' + \frac{G_i A_{gi}}{f_{si}} (v_i' - \beta_i') = 0 \quad \text{or} \quad \delta v_i = 0. \tag{6b}$$

By eliminating β_i from equation (5), partial differential equation of motion for vertical free vibration can be obtained as follows:

$$m_i \ddot{v}_i + E_{gi} I_{gi} v_i'''' - (\rho_{gi} I_{gi} + \underline{S_i m_i}) \ddot{v}_i'' + S_{\rho_i} m_i \ddot{v}_i - H_w v_i'' + \frac{m_i g}{H_w} H(t) + \underline{S_i H_w} v_i'''' - S_{\rho_i} \left(H_w \ddot{v}_i'' - \frac{m_i g}{H_w} \ddot{H}(t) \right) = 0, \tag{7}$$

where

$$S_i = f_{si} \frac{E_{gi} I_{gi}}{G_i A_{gi}}, \quad S_{\rho i} = f_{si} \frac{\rho_{gi} I_{gi}}{G_i A_{gi}}. \quad (8)$$

The underlined three terms in equation (7) denote the terms neglected in the previous studies [3, 6]. The following equation of boundary condition at each end of the girder ($x_i = 0, l_i$) for a suspension bridge with simply supported stiffening girder can be obtained from equation (5a) by substituting the condition ($\beta'_i = 0$) that the bending moment is zero at the ends of the girder:

$$H_w v'_i - \frac{m_i g}{H_w} H(t) + \frac{G_i A_{gi}}{f_{si}} v''_i = 0. \quad (9)$$

If additional cable tension $H(t)$ or shear coefficient f_{si} is zero, equation (9) becomes $v'_i = 0$ at the ends of the girder.

4. ANALYTICAL SOLUTION FOR HINGED SINGLE-SPAN SUSPENSION BRIDGE

In this section, analytical solution for natural frequencies and mode shapes of a hinged single-span suspension bridge are derived. Subscript i denoting i th span is omitted in this section.

4.1. SYMMETRIC MODE

Partial differential equation of motion for a hinged single-span suspension bridge can be rewritten in the following form

$$m\ddot{v} + E_g I_g v'''' - (\rho_g I_g + Sm)\ddot{v}'' + S_\rho m\ddot{v} - H_w v'' + \frac{mg}{H_w} H(t) + SH_w v'''' - S_\rho H_w \ddot{v}'' + S_\rho \frac{mg}{H_w} \dot{H}(t) = 0, \quad (10a)$$

$$H(t) = \frac{E_c A_c}{L_E} (u(l) - u(0)) + \frac{E_c A_c}{L_E} \frac{mg}{H_w} \int_0^l v \, dx. \quad (10b)$$

The equations of boundary condition can be obtained from equations (6b) and (9).

$$v(0) = v(l) = 0, \quad (11a)$$

$$\left(H_w + \frac{GA_g}{f_s} \right) v''(0) - \frac{mg}{H_w} H(t) = 0, \quad (11b)$$

$$\left(H_w + \frac{GA_g}{f_s} \right) v''(l) - \frac{mg}{H_w} H(t) = 0. \quad (11c)$$

Longitudinal displacement at each end of the cable, vertical displacement and the additional cable tension can be assumed as follows:

$$u(0, t) = u_0 e^{i\omega_n t}, \quad u(l, t) = u_l e^{i\omega_n t}, \quad v(x, t) = \phi_n(x) e^{i\omega_n t}, \quad H(t) = h e^{i\omega_n t}, \quad (12)$$

where ω_n is the natural frequency of the n th symmetric mode. Substituting equation (12) into equation (10), the following ordinary differential equation is obtained:

$$a_1 \phi_n'''' - 2a_2 \phi_n'' - a_3 \phi_n + a_4 h = 0, \quad (13a)$$

$$h = \frac{E_c A_c}{L_E} (u_l - u_0) + \frac{E_c A_c}{L_E} \frac{mg}{H_w} \int_0^l \phi_n dx, \quad (13b)$$

where

$$a_1 = E_g I_g + S H_w, \quad a_2 = \frac{1}{2} [H_w - (\rho_g I_g + S m + S_\rho H_w) \omega_n^2] \quad (14)$$

$$a_3 = m \omega_n^2 - S_\rho m \omega_n^4, \quad a_4 = \frac{mg}{H_w} - \frac{mg}{H_w} S_\rho \omega_n^2.$$

Substituting equation (12) into equation (11), equations of boundary condition are also given as

$$\phi_n(0) = \phi_n(l) = 0, \quad (15a)$$

$$(S H_w + E_g I_g) \phi_n''(0) - \frac{mg}{H_w} S h = 0, \quad (15b)$$

$$(S H_w + E_g I_g) \phi_n''(l) - \frac{mg}{H_w} S h = 0. \quad (15c)$$

Suppose that h in equation (13a) is constant, general solution of equation (13a) can be expressed as

$$\phi_n(x) = h [c_1 \sinh(\lambda x) + c_2 \cosh(\lambda x) + c_3 \sin(\mu x) + c_4 \cos(\mu x) + D] \quad (16a)$$

where

$$\lambda^2 = \frac{a^2 + \sqrt{a_2^2 + a_1 a_3}}{a_1}, \quad \mu^2 = \frac{-a_2 + \sqrt{a_2^2 + a_1 a_3}}{a_1}. \quad (16b)$$

The following integral constants are obtained by substituting equation (16) into equation (15):

$$c_1 = -\tanh\left(\frac{\lambda l}{2}\right) \frac{P - D\mu^2}{\lambda^2 + \mu^2}, \quad c_2 = \frac{P - D\mu^2}{\lambda^2 + \mu^2} \quad (17)$$

$$c_3 = \tan\left(\frac{\mu l}{2}\right) \frac{P + D\lambda^2}{\lambda^2 + \mu^2}, \quad c_4 = -\frac{P + D\lambda^2}{\lambda^2 + \mu^2}, \quad P = \frac{mg f_{si}}{f_{si} H_w + G A_g H_w}, \quad D = \frac{a_4}{a_3}.$$

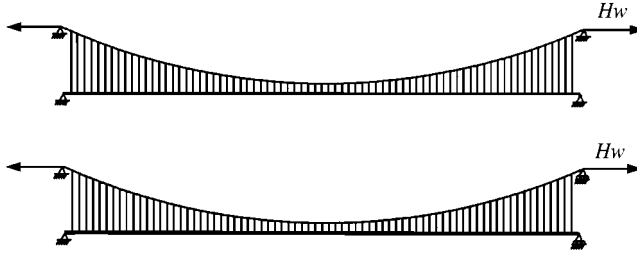


Figure 1. Configuration of simply supported single-span suspension bridge: (a) hinge-hinge support; (b) hinge-roller support.

In the case of a suspension bridge as shown in Figure 1, the characteristic equation can be obtained by substituting equation (16a) into equation (13b) and then integrating,

$$\frac{L_E}{E_c A_c} = \frac{mg/H_w}{\lambda^2 + \mu^2} \left[Dl(\lambda^2 + \mu^2) + \frac{2(P - D\mu^2)}{\lambda} \tanh\left(\frac{\lambda l}{2}\right) - \frac{2(P + D\lambda^2)}{\mu} \tan\left(\frac{\mu l}{2}\right) \right]. \quad (18)$$

Finally, the natural frequency can be obtained by solving the n th solution of equation (18) and the mode shape is easily obtained by substituting the obtained natural frequency into equation (16a).

4.2. ANTISYMMETRIC MODE

The vibration in antisymmetric mode causes no additional cable tension $H(t)$ because the upward and the downward deflections on each side of the centerline balance with each other. By applying this condition to equations (10) and (11), equation of motion and boundary condition can be found to be as follows:

$$m\ddot{v} + E_g I_g v'''' - (\rho_g I_g + Sm)\dot{v}'' + S_\rho m \ddot{v} - H_w v'' + SH_w v'''' - S_\rho H_w \dot{v}'' = 0, \quad (19a)$$

$$v(0) = v(l) = v''(0) = v''(l) = 0. \quad (19b)$$

The solution of equation (19) can be assumed as follows:

$$v(x, t) = \sin(\lambda_n x) e^{i\omega_n t}, \quad (20a)$$

where

$$\lambda_n = \frac{2n\pi}{l} \quad (20b)$$

and ω_n is the natural frequency of the n th antisymmetric mode. Substituting equation (20) into equation (19a) the following characteristic equation is obtained:

$$E_g I_g \lambda_n^4 - \rho_g I_g \lambda_n^2 \omega_n^2 + (H_w \lambda_n^2 - m \omega_n^2)(1 + S \lambda_n^2 - S_\rho \omega_n^2) = 0. \quad (21)$$

Finally, natural frequency can be obtained by solving the n th solution of equation (21) and the mode shape is obtained by substituting the obtained natural frequency into equation (20).

In the case of a single-span suspension bridge with hinge-roller support shown in Figure 1(b), the symmetric mode also causes no additional cable tension $H(t)$ due to the freely movable boundary condition at horizontal direction. That is,

$$H(t) = 0 = u(l) + \frac{pE_c A_c}{L_E} \int_0^l v \, dx. \quad (22)$$

Therefore, natural frequencies of a single-span suspension bridge with a hinge-roller support corresponding to the symmetric mode with zero additional cable tension can be evaluated by inserting equation (23) into equation (21) and solving equation (21). These modes are considered while calculating the analytical solutions of hinged three-span suspension bridge in sections 5.2 and 5.3:

$$\lambda_n = \frac{(2n - 1)\pi}{l}. \quad (23)$$

5. ANALYTICAL SOLUTION FOR HINGED THREE-SPAN SUSPENSION BRIDGE

In this section, the results in section 4 are extended to a hinged three-span suspension bridge and the analytical solution for natural frequencies and mode shapes are presented. (see Figure 2).

5.1. SYMMETRIC MODE

Partial differential equation of motion for a hinged three-span suspension bridge are given as equations (7) and (4). In the same manner as in section 4.1, the equations of boundary condition for each span can be expressed in the same form as equation (11). In the case of symmetric vibration, the first term on the right-hand side of equation (4) vanishes because of $\sum_{i=1}^3 [u_i(l_i) - u_i(0)] = 0$. The longitudinal displacement at each end of the cable, vertical displacement and additional component of cable tension can be assumed as follows:

$$u_i(0, t) = u_{i0} e^{i\omega_n t}, \quad u_i(l_i, t) = u_i e^{i\omega_n t}, \quad v_i(x_i, t) = \phi_{in}(x) e^{i\omega_n t}, \quad H(t) = h e^{i\omega_n t}. \quad (24)$$

Finally, the following ordinary differential equation for the i th span is obtained:

$$a_{1i} \phi_{in}'''' - 2a_{2i} \phi_{in}'' - a_{3i} \phi_{in} + a_{4i} h = 0, \quad (25a)$$

$$h = \frac{E_c A_c}{L_E} \sum_{i=1}^3 \frac{m_i g}{H_w} \int_0^{l_i} \phi_{in} \, dx_i, \quad (25b)$$

where the coefficients a_{1i} , a_{2i} , a_{3i} and a_{4i} for the i th span is the same as in equation (14).

Equation (25) can be solved in the same manner as in section 4. The general solution of equation (25a) can be expressed as

$$\phi_{in}(x) = h [c_{1i} \sinh(\lambda_i x_i) + c_{2i} \cosh(\lambda_i x_i) + c_{3i} \sin(\mu_i x_i) + c_{4i} \cos(\mu_i x_i) + D_i], \quad (26)$$

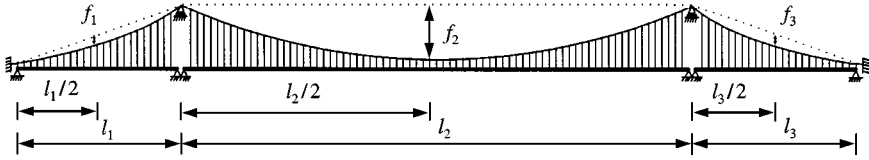


Figure 2. Configuration of three-span suspension bridge.

where the coefficients c_{1i} , c_{2i} , c_{3i} and c_{4i} are defined at span by span and have the same form as equation (17). In the case of a hinged three-span suspension bridges, the characteristic equation can be obtained by substituting equation (26) into equation (25b) and then integrating:

$$\frac{L_E}{E_c A_c} = \sum_{i=1}^3 \frac{m_i g}{H_w} \frac{1}{\lambda_i^2 + \mu_i^2} \left(D_i l_i (\lambda_i^2 + \mu_i^2) + \frac{2(P_i - D_i \mu_i^2)}{\lambda_i} \tanh\left(\frac{\lambda_i l_i}{2}\right) - \frac{2(P_i + D_i \lambda_i^2)}{\mu_i} \tan\left(\frac{\mu_i l_i}{2}\right) \right). \quad (27)$$

Consequently, natural frequencies and mode shapes causing additional cable tension can be obtained from equations (27) and (26). On the contrary, it is possible that the globally symmetric but locally antisymmetric modes in the side span give no additional tension. Frequencies of these antisymmetric modes in the side span coincide with those corresponding to globally as well as locally antisymmetric modes given in the next section (see the 5th and the 10th modes in Figure 5).

5.2. ANTISYMMETRIC MODE

As already mentioned in section 4.2, the locally antisymmetric modes in the center and the side span, respectively, cause no additional cable tension. Consequently, there is no interaction between center span and side span in these modes. That is, independent vibration modes are possible at each span. The equation of motion and boundary conditions can be found to be as follows:

$$m_i \ddot{v}_i + E_{gi} I_{gi} v_i'''' - (\rho_{gi} I_{gi} + S_i m_i) \ddot{v}_i'' + S_{\rho i} m_i v_i'' - H_w v_i' + S_i H_w v_i'''' - S_{\rho i} H_w \ddot{v}_i'' = 0, \quad (28a)$$

$$v_i(0) = v_i(l_i) = v_i''(0) = v_i''(l_i) = 0. \quad (28b)$$

In the same manner as in section 4.2, mode shape and the characteristic equation can be expressed as follows:

$$v_i(x_i, t) = \sin(\lambda_n x_i) e^{i\omega_n t}, \quad (29a)$$

$$E_{gi} I_{gi} \lambda_n^4 - \rho_{gi} I_{gi} \lambda_n^4 \omega_{in}^2 - (H_w \lambda_n^2 - m_i \omega_{in}^2)(1 + S_i \lambda_n^2 - S_{\rho i} \omega_{in}^2) = 0, \quad (29b)$$

where ω_{in} is the n th antisymmetric natural frequency of the i th span.

On the contrary, it is possible that the globally antisymmetric but locally symmetric modes in the side span also give no additional tension (see the 2nd and the 7th antisymmetric modes in Figure 5). Frequencies corresponding to these symmetric modes in the side span can be evaluated from equations (22) and (23).

5.3. ANALYTICAL SOLUTION PROCEDURE

Based on the scheme presented in sections 5.1 and 5.2, the procedures for determining the globally symmetric and antisymmetric vibration modes and frequencies can be summarized as follows:

- (1) Calculate the natural frequencies corresponding to globally symmetric modes from equations (27) and (26).
- (2) By substituting $\lambda_n = 2n\pi/l$ and $i = 2$ into equation (29), evaluate the natural frequencies corresponding to antisymmetric modes of the center span only.
- (3) By substituting $\lambda_n = 2n\pi/l$ and $i = 1$ into equation (29), evaluate the natural frequencies corresponding to antisymmetric modes of the side span only.
- (4) Substituting $\lambda_n = (2n - 1)\pi/l$ and $i = 1$ into equation (29), obtain the natural frequencies corresponding to symmetric modes of the side span only. It should be noted that these modes add no additional tension.
- (5) For determining globally symmetric modes, rearrange the natural frequencies calculated at steps (1) and (3) in the descending order. The mode shapes of third span corresponding to step (3) are obtained by drawing a mirror image of the first span.
- (6) For determining globally antisymmetric modes, rearrange the natural frequencies calculated in steps (2)–(4) in the descending order. The mode shapes corresponding to steps (3) and (4) are obtained by drawing modes of the third span antisymmetrically with respect to the center span.

6. ANALYTICAL SOLUTION FOR CONTINUOUS THREE-SPAN SUSPENSION BRIDGE

The rotational displacement can be assumed as follows:

$$\beta_i(x_i, t) = \varphi_i(x)e^{i\omega t}. \quad (30)$$

Rearranging the equation of motion of equation (5), the following equation of motion can be obtained:

$$\left(H_w + \frac{G_i A_{gi}}{f_{si}}\right) \phi_i'' + m_i \omega^2 \phi_i - \frac{G_i A_{gi}}{f_{si}} \phi_i' - \frac{m_i g}{H_w} h = 0, \quad (31a)$$

$$S_i \phi_i'' - (1 - \omega^2 S_{\rho i}) \phi_i + \phi_i' = 0. \quad (31b)$$

Natural and geometrical boundary conditions are found to be as follows:

$$\begin{aligned} \phi_i(0) = \phi_i(l_i) = 0, \quad E_{g1} I_{g1} \phi_1'(0) = E_{g3} I_{g3} \phi_3'(l_i) = 0, \\ \phi_1(l_1) = \phi_2(0), \quad E_{g1} I_{g1} \phi_1'(l_1) = E_{g2} I_{g2} \phi_2'(0), \\ \phi_2(l_2) = \phi_3(0), \quad E_{g2} I_{g2} \phi_2'(l_2) = E_{g3} I_{g3} \phi_3'(0). \end{aligned} \quad (32)$$

The general solution for translational and rotational mode shape can be expressed as

$$\phi_{in}(x) = h [c_{1i} \sinh(\lambda_i x_i) + c_{2i} \cosh(\lambda_i x_i) + c_{3i} \sin(\mu_i x_i) + c_{4i} \cos(\mu_i x_i)] + \frac{g}{\omega^2 H_w} h, \quad (33a)$$

$$\varphi_{in}(x) = h [d_{1i} \sinh(\lambda_i x_i) + d_{2i} \cosh(\lambda_i x_i) + d_{3i} \sin(\mu_i x_i) + d_{4i} \cos(\mu_i x_i)]. \quad (33b)$$

The following integral constants for the the rotational mode shapes are obtained in terms of integral constants for the translational mode shapes:

$$\begin{aligned} d_{1i} &= \frac{c_{2i}\lambda_i}{(1 - \omega^2 S_{\rho i}) - S_i \lambda_i^2}, & d_{2i} &= \frac{c_{1i}\lambda_i}{(1 - \omega^2 S_{\rho i}) - S_i \lambda_i^2}, \\ d_{3i} &= \frac{-c_{4i}\mu_i}{(1 - \omega^2 S_{\rho i}) + S_i \mu_i^2}, & d_{4i} &= \frac{c_{3i}\mu_i}{(1 - \omega^2 S_{\rho i}) + S_i \mu_i^2}. \end{aligned} \quad (34)$$

In the case of continuous suspension bridges, the scheme developed by Hayashikawa [6] can be used for determining the integral constants and natural frequencies.

7. SUSPENSION BRIDGE ELEMENT

The stiffness and mass matrices of suspension bridge elements considering the effects of both shear deformation and rotary inertia are derived in this section.

7.1. SHAPE FUNCTION CONSIDERING SHEAR DEFORMATION

In finite element approach, the suspension bridge is assumed to be divided into a system of discrete elements. It has been assumed previously that hangers are inextensible and remain vertical during vibration and that consequently the vibrational displacements of both the cable and the stiffening girder are identical. If only vertical displacements are considered, there are two nodal-degrees-of-freedom (d.o.f.) at each node: translational and rotational displacement (Figure 3). The interpolation functions associated with the two nodal-d.o.f. are assumed to be cubic Hermitian polynomials considering shear deformation. Using the element displacement vector, vertical and rotational displacement are interpolated as follows:

$$v = h_1 v^p + h_2 l w^p + h_3 v^q + h_4 l w^q, \quad (35a)$$

$$l\beta = k_1 v^p + k_2 l w^p + k_3 v^q + k_4 l w^q, \quad (35b)$$

where

$$\begin{aligned} h_1 &= (2\gamma^3 - 3\gamma^2 - 12S_e\gamma + 1 + 12S_e)/(1 + 12S_e), \\ h_2 &= \{\gamma^3 - 2(1 + 3S_e)\gamma^2 + (1 + 6S_e)\gamma\}/(1 + 12S_e), \\ h_3 &= (-2\gamma^3 + 3\gamma^2 + 12S_e\gamma)/(1 + 12S_e), \\ h_4 &= \{\gamma^3 - (1 - 6S_e)\gamma^2 - 6S_e\gamma\}/(1 + 12S_e), \\ k_1 &= (6\gamma^2 - 6\gamma)/(1 + 12S_e), \\ k_2 &= \{3\gamma^2 - 4(1 + 3S_e)\gamma^2 - 1 + 12S_e\}/(1 + 12S_e), \\ k_3 &= (-6\gamma^3 + 6\gamma)/(1 + 12S_e), \\ k_4 &= \{3\gamma^2 - 2(1 - 6S_e)\gamma\}/(1 + 12S_e), \\ S_e &= \frac{f_s E_g I_g}{G_g A_g l^2}, & \gamma &= \frac{x}{l}. \end{aligned} \quad (36)$$

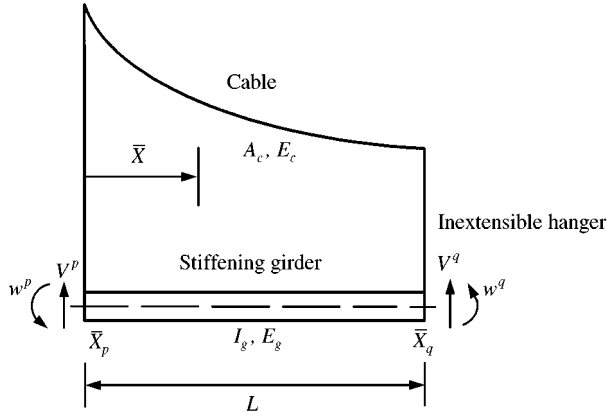


Figure 3. Displacement vector of suspension bridge element.

7.2. STIFFNESS AND MASS MATRICES OF THE SUSPENSION BRIDGE ELEMENT

The following kinetic and potential energy with respect to nodal displacement vector \mathbf{V}_e can be obtained by substituting equation (35) into equation (2) and integrating:

$$T = \sum_{e=1}^n \frac{1}{2} \mathbf{V}_e^T \mathbf{M}_e \mathbf{V}_e, \quad (37a)$$

$$V = \sum_{e=1}^n \frac{1}{2} \mathbf{V}_e^T (\mathbf{K}_{cg}^e + \mathbf{K}_{eg}^e) \mathbf{V}_e + \frac{1}{2} \frac{H^2(t) L_E}{E_c A_c}, \quad (37b)$$

where n is the total number of elements.

\mathbf{M}_e , \mathbf{K}_{cg}^e , \mathbf{K}_{eg}^e are the consistent-mass matrix, the element gravity-stiffness matrix of the cable and the element elastic stiffness matrix of the stiffening girder considering both shear deformation and rotary inertia respectively. The resulting matrices are listed in Appendix A

Applying the shape function to equation (4), additional horizontal component of cable tension can be expressed as

$$H(t) = \frac{E_c A_c}{L_E} \sum_e \frac{mg}{H_w} \mathbf{f}_e^T \mathbf{V}_e, \quad (38)$$

where \mathbf{f}_e^T is the vector of the polynomials integrating shape function which may be expressed as

$$\mathbf{f}_e^T = \frac{1}{T} \left[l \left(\frac{1}{2} + 6S_e \right), \quad l^2 \left(\frac{1}{12} + S_e \right), \quad l \left(\frac{1}{2} + 6S_e \right), \quad -l^2 \left(\frac{1}{12} + S_e \right) \right]. \quad (39)$$

Using the equation (38), the second term on right-hand side of equation (37b) can be written as

$$\frac{1}{2} \frac{H^2(t) L_E}{E_c A_c} = \frac{1}{2} \mathbf{U}^T \mathbf{K}_{CE} \mathbf{U}, \quad (40a)$$

$$\mathbf{K}_{CE} = \frac{E_c A_c}{L_E} \left[\left(\sum_e \frac{mg}{H_w} \mathbf{f}_e \right) \left(\sum_e \frac{mg}{H_w} \mathbf{f}_e \right)^T \right], \quad (40b)$$

TABLE 2

Buckling load (kN) for various truss type, L = 100 m

		Type 1	Type 2	Type 3	Type 4	Type 5	Type 6
Equation (42)	Shear ignored	158067.9	158067.9	158067.9	158067.9	158067.9	158067.9
	Shear considered	133657.6	136815.1	136815.1	146675.7	146675.7	136227.0
	Full truss model	133595.5	136390.4	137253.5	147302.7	147237.5	135985.8

in which \mathbf{U} is the global nodal displacement and \mathbf{K}_{CE} is the global elastic stiffness matrix of the cable. Stiffness matrix is a full matrix, i.e., not banded. This means that an interaction exists not only between adjacent elements but also among all elements of the structure. By inserting equation (37) into Hamilton's principle and by applying the variational operator, the matrix equation of motion for the assemblage can be obtained in the following form:

$$\mathbf{M}\ddot{\mathbf{U}} + (\mathbf{K}_{EG} + \mathbf{K}_{CG} + \mathbf{K}_{CE})\mathbf{U} = 0, \quad (41)$$

in which \mathbf{M} is the global consistent mass matrix, \mathbf{K}_{EG} and \mathbf{K}_{CG} are the global stiffness matrix of the stiffening girder and the global gravity stiffness matrix of the cable.

8. NUMERICAL EXAMPLES

In order to demonstrate the validity of the present equivalent beam with shear coefficient in Table 1, the stability of the truss girder is investigated. The structural properties of the truss girder are given as follows. $E = 2.05 \times 10^8$ kPa, $G = 78.86 \times 10^6$ kPa, $A = 0.125$ m², $A_d = 0.01404$ m², $A_v = 0.02825$ m², mass per unit length of upper and bottom chord = 0.505102 t/m, mass per unit length of diagonal member = 0.112245 t/m and the mass per unit length of vertical member = 0.220408 t/m. The buckling load based on Timoshenko's beam theory is as follows:

$$P_{cr} = \frac{\pi^2 EI}{L^2 + (\pi^2 f_s EI/GA)}. \quad (42)$$

Buckling load for various truss girder types listed in Table 1 are shown in Table 2. It is noted that little difference is observed between buckling load evaluated from equation (42) considering shear effects and buckling load analyzed with the full truss model.

Numerical examples for suspension bridge in Figure 4 are presented to demonstrate the effectiveness of analytical and numerical solution developed herein. Comparisons with the full truss model of suspension bridges are made. The full truss model represents that each members of truss, cable and hanger are modelled by the truss element. The geometry and structural properties of the numerical example bridge are given as follows [12]:

- (1) *Stiffening truss*: $l_1 = l_3 = 250$ m, $l_2 = 770$ m, $A_1 = A_3 = 0.10$ m², $A_2 = 0.12$ m², $A_d = 0.030$ m², $A_v = 0.015$ m², $w_{g1} = w_{g3} = 73.575$ kN/m, $w_{g2} = 76.518$ kN/m, $f_{s1} = f_{s3} = 3.807$, $f_{s2} = 4.634$, $E_{g1} = E_{g2} = E_{g3} = 2.06 \times 10^8$ kPa, $G_{g1} = G_{g2} = G_{g3} = 7.923 \times 10^7$ kPa.
- (2) *Cable*: cable sag length $f_1 = f_3 = 7.849$ m, $f_2 = 75.95$ m, $A_c = 0.250$ m², $E_c = 1.962 \times 10^8$ kPa, $w_{c1} = w_{c3} = 24.525$ kN/m, $w_{c2} = 23.544$ kN/m.
 - hanger: $A_h = 0.006$ m², $E_h = 1.373 \times 10^8$ kPa.
 - single-span bridge: $H_w = 9.7641 \times 10^4$ kN, $L_E = 829.93$ m.
 - three-span bridge: $H_w = 9.7641 \times 10^4$ kN, $L_E = 1357.29$ m.

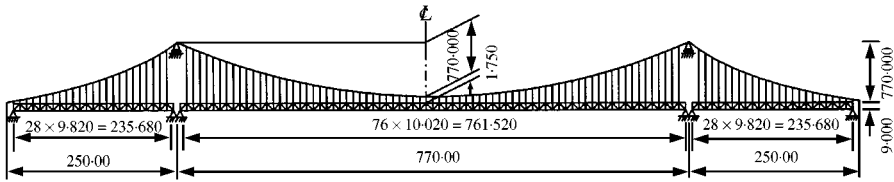


Figure 4. Configuration of three-span suspension bridge of vertical vibration.

TABLE 3
Natural frequencies of hinged single-span suspension bridge

Mode	This study					
	Analytical sol.		Numerical sol.		Full truss model	
	Symmetric	Antisymmetric	Symmetric	Antisymmetric	Symmetric	Antisymmetric
1	1.45492 (1.46571)	0.93516 (0.93762)	1.45497 (1.46571)	0.93516 (0.93762)	1.45612	0.93248
2	2.16967 (2.17617)	2.44887 (2.49918)	2.16975 (2.17617)	2.44924 (2.49919)	2.15275	2.43022
3	3.50520 (3.63048)	4.66224 (4.92835)	3.50664 (3.63052)	4.66654 (4.92848)	3.35579	4.68467
4	6.00908 (6.49619)	7.47258 (8.28579)	6.01947 (6.49652)	7.49443 (8.28654)	6.00744	7.44526
5	9.05841 (10.3206)	10.7338 (12.5877)	9.09966 (10.3221)	10.8056 (12.5906)	8.99266	10.4694
6	12.4921 (15.0956)	14.3129 (17.8392)	12.6089 (15.1008)	14.4930 (17.8480)	12.4292	14.1502
7	16.1884 (20.8224)	18.1050 (24.0425)	16.4541 (20.8367)	18.4824 (24.0648)	15.9179	18.1974
8	20.0564 (27.5017)	22.0333 (31.1985)	20.5757 (27.5354)	22.7288 (31.2481)	19.5490	21.2664
9	24.0313 (35.1341)	26.0442 (39.3077)	24.9408 (35.2052)	27.2093 (39.4074)	22.9036	24.4833
10	28.0690 (43.7199)	30.1015 (48.3702)	29.5345 (43.8572)	31.9152 (48.5561)	25.8560	27.8090

Note: (), shear neglected.

Natural frequencies of a hinged single-span suspension bridge are given in Table 3 for three different methods, (1) the analytical solution, (2) the numerical solution using suspension bridge element, and (3) the numerical solution using the full truss model. Data of the center span is taken for analysis. Whether shear deformation and rotary inertia are ignored or not, the results of the analytical solution are almost identical to those of the numerical solution. It can be seen that the effect of shear deformation and rotary inertia on natural frequencies is increased as the mode become higher. In the case of considering shear effects, the analytical solution as well as the numerical solution show good agreement with the full truss model.

TABLE 4

Natural frequencies of hinged three-span suspension bridge

Mode	This study					
	Analytical sol.		Numerical sol.		Full truss model	
	Symmetric	Antisymmetric	Symmetric	Antisymmetric	Symmetric	Antisymmetric
1	1·12667 (1·13228) [‡]	0·92232 (0·92466)	1·12669 (1·13228)	0·92232 (0·92466)	1·19845	0·93237
2	1·59586 (1·60976)	1·68906 (1·70312)	1·59591 (1·60977)	1·68908 (1·70312)	1·68899	1·95969
3	2·37095 (2·38127)	2·40782 (2·45584)	2·37101 (2·38127)	2·40818 (2·45585)	2·43585	2·46388
4	3·43330 (3·55351)	4·57879 (4·83341)	3·43469 (3·55354)	4·58292 (4·83354)	3·51519	4·59604
5	4·87408* (5·13028)	4·87408* (5·13028)	4·87589 (5·13030)	4·87589 (5·13030)	4·95307	4·95349
6	5·89822 (6·36506)	7·33822 (8·11806)	5·90821 (6·36538)	7·35926 (8·11880)	6·00492	7·73951
7	8·89596 (10·1077)	9·47146 [†] (10·6962)	8·93574 (10·1092)	9·48912 (10·6965)	8·99668	9·83994
8	9·48009 [†] (10·7039)	10·5448 (12·3261)	9·49773 (10·7042)	10·6141 (12·3290)	9·88493	10·5145
9	12·2751 (14·7789)	14·0688 (17·4628)	12·3880 (14·7840)	14·2433 (17·4715)	12·2493	14·1678
10	15·0137* (18·4596)	15·0137* (18·4596)	15·0922 (18·4614)	15·0922 (18·4614)	14·5921	14·5980

Note: *, zero additional cable tension mode; †, close-to-zero additional cable tension mode; ‡ (), shear neglected.

Applying the procedure listed in section 5.3, the natural frequencies of hinged three-span suspension bridge are given in Table 4, while Figure 5 shows the mode shapes of vertical vibration. Similar to the results of single-span suspension bridge, the effect of shear deformation and rotary inertia is shown to become greater with higher modes.

Furthermore, it is interesting to point out that the characteristic equation can have double roots of eigenvalues. As shown in Table 4 and Figure 5, natural frequencies corresponding to the 5th and the 10th symmetric and antisymmetric modes coincide with double roots and these corresponding modes create no tension increment because of locally antisymmetric mode shape in the side span (see scheme (3) in section 5.3).

On the other hand, the 2nd and 7th antisymmetric modes in Figure 5 correspond to the globally antisymmetric but locally symmetric mode (see scheme (4) in section 5.3). It should be noted that these mode do not create any additional horizontal component of cable tension because the symmetric mode in the side span corresponds to the higher-roller or roller-hinged support. However, the 2nd and 8th symmetric modes in Figure 5 correspond to the globally and locally symmetric mode. The difference between the globally antisymmetric but locally symmetric mode and the globally and locally symmetric mode can be expressed as in Figure 6. As shown in Figure 6, the mode shapes of side span can be


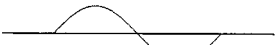
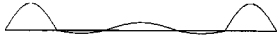
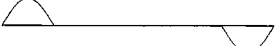
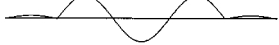
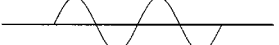
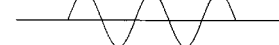
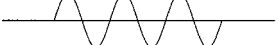
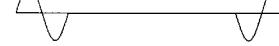

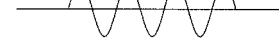
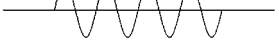
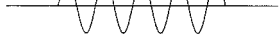


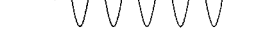
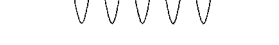
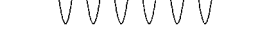
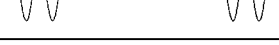
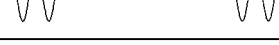
No.	Symmetric mode	(rad/s)	Antisymmetric mode	(rad/s)
1		1.12667		0.92232
2		1.59586 [†]		1.68906 [†]
3		2.37095		2.40782
4		3.43330		4.57879
5		4.87408 [*]		4.87408 [*]
6		5.89822		7.33822
7		8.89596		9.47146 [†]
8		9.48009 [†]		10.5448
9		12.2751		14.0688
10		15.0137 [*]		15.0137 [*]

Figure 5. Mode shapes of vertical vibration of hinged three-span suspension bridge.

categorized in 3 cases due to its freely movable boundary condition. Figure 6(a) corresponds to the globally antisymmetric but locally symmetric mode, and Figure 6(b) and 6(c) correspond to the globally and locally symmetric mode. The former is named as “zero additional cable tension mode” and the latter is named as “close-to-zero additional cable tension mode”. Because of the globally symmetric mode, minor tension change occurs at the center span in Figure 6(b) and 6(c). The natural frequencies of the 2nd symmetric and antisymmetric modes, and the 8th symmetric and the 7th antisymmetric modes in Figure 5 do not coincide with each other due to this tension change in the center span. A greater difference can be found in the natural frequencies of the 2nd symmetric and antisymmetric modes.

Other symmetric and antisymmetric modes in Figure 5 can be evaluated using schemes (1) and (2) in section 5.3 respectively.

Some of the computed natural frequencies of the continuous three span type are presented for the first 10 modes of the symmetric and antisymmetric vibrations in Table 5. Similar to the results of hinged suspension bridge, the present study shows good agreement with the full truss model especially at higher modes. Also the effect of shear deformation and rotary inertia is shown to become greater with higher modes. The values of the natural

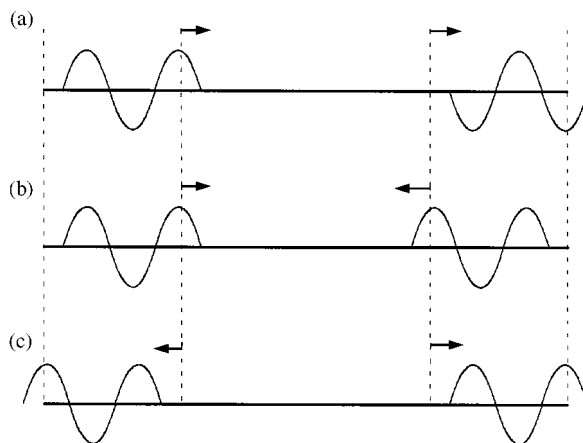


Figure 6. Locally symmetric mode in side span of hinged three-span suspension bridge.

TABLE 5

Natural frequencies of continuous three-span suspension bridge

Mode	This study					
	Analytical sol.		Numerical sol.		Full truss model	
	Symmetric	Antisymmetric	Symmetric	Antisymmetric	Symmetric	Antisymmetric
1	1.19457 (1.20842)	0.99665 (1.00337)	1.19463 (1.20842)	0.99667 (1.00337)	1.22351	1.01393
2	1.61630 (1.63301)	1.89504 (1.92992)	1.61637 (1.63301)	1.89512 (1.92992)	1.69679	2.03080
3	2.52958 (2.56418)	2.62593 (2.71981)	2.52969 (2.56418)	2.62651 (2.71983)	2.56266	2.60304
4	3.63790 (3.80274)	4.65952 (4.92220)	3.63961 (3.80279)	4.66337 (4.92230)	3.63341	4.61753
5	5.22110 (5.59276)	5.41971 (5.91485)	5.22411 (5.59283)	5.42376 (5.91495)	5.18252	5.33341
6	6.23418 (6.89647)	7.58085 (8.51489)	6.24578 (6.89685)	7.60407 (8.51571)	6.18213	7.62772
7	9.02503 (10.2748)	9.85018 (11.3654)	9.06323 (10.2761)	9.87552 (11.3662)	8.99860	9.79892
8	10.0578 (11.8650)	10.9059 (13.1414)	10.0861 (11.8660)	10.9785 (13.1444)	10.4463	10.8769
9	12.5248 (15.3538)	14.2289 (17.7336)	12.6437 (15.3592)	14.4011 (17.7412)	12.2455	14.6369
10	15.3479 (19.2987)	15.5106 (19.9589)	15.4524 (19.3034)	15.6133 (19.9640)	14.8506	15.7789

Note: (), shear neglected.

frequencies of continuous three-span suspension bridges are generally larger than those of hinged three-span suspension bridges. The difference between them is clearly represented by their respective boundary conditions for the stiffening girders.

9. CONCLUSION

This study develops an analytical and numerical method for free vertical vibration of suspension bridges including shear deformation and rotary inertia. By applying Hamilton's principle, the differential equation of motion and boundary condition are derived from the kinetic and potential energy of the cable and stiffening girder. Three new terms which were neglected in previous studies are included in this study. General solutions for free vertical vibrations are presented for finding natural frequencies and mode shapes of single- and three-span suspension bridges. For finite element analysis, the shear flexible suspension bridge element is developed by using Hermitian polynomials considering shear deformation effects.

Detailed numerical examples are provided to illustrate the applicability and effectiveness of the present method. Furthermore, rigorous comparison with full truss model has been made. A substantial difference in frequencies of higher mode was found when compared with a case in which (1) the shear deformation and rotary inertia was taken into consideration and (2) a case in which the shear deformation and rotary inertia was not taken into consideration. It can be concluded that the effects of shear deformation and rotary inertia should not be neglected for computing natural frequencies of higher modes. In addition, it should be pointed out that double-root frequencies corresponding to the globally symmetric and antisymmetric modes, respectively, can occur in the hinged three-span suspension bridges and also, the globally antisymmetric but locally symmetric modes in side span which create no tension change can be found.

REFERENCES

1. D. B. STEINMAN 1935 *Transaction of ASCE* **100**, A generalized deflection theory for suspension bridges.
2. F. BLEICH, C. B. MCCULLOUGH, R. ROSECRANS and G. S. VINCENT 1950 *The Mathematical Theory of Vibration in Suspension Bridges*. Washington, DC.: US Bureau of Public Roads, Government Printing Office.
3. A. M. ABDEL-GHAFFAR 1980 *ASCE Journal of Structural Division* **106**, 2053–2075. Vertical vibration analysis of suspension bridges.
4. A. M. ABDEL-GHAFFAR 1979 *ASCE Journal of Structural Division* **105**, 767–788. Free torsional vibrations of suspension bridges.
5. A. M. ABDEL-GHAFFAR 1978 *ASCE Journal of Structural Division* **104**, 503–525. Free lateral vibrations of suspension bridges.
6. T. HAYASHIKAWA and N. WATANABE 1982 *ASCE Journal of Engineering Mechanics Division* **110**, 341–356. Vertical vibration in Timoshenko beam suspension bridges.
7. T. HAYASHIKAWA 1997 *Journal of Sound and Vibration* **204**, 117–129. Torsional vibration analysis of suspension bridges with gravitational stiffness.
8. S. P. TIMOSHENKO and J. M. GERE 1961 *Theory of Elastic Stability*. New York: McGraw-Hill.
9. A. K. CHUGH 1977 *International Journal for Numerical Methods in Engineering* **2**, 1681–1697. Stiffness matrix for a beam element including transverse shear and axial force effects.
10. M. Y. KIM, S. P. CHANG and S. B. KIM 1994 *International Journal for Numerical Methods in Engineering* **37**, 4097–4115. Spatial stability and free vibration of shear flexible thin-walled elastic beams. I: analytical approach.
11. M. Y. KIM, S. P. CHANG and S. B. KIM 1994 *International Journal for Numerical Methods in Engineering* **37**, 4117–4140. Spatial stability and free vibration of shear flexible thin-walled elastic beams. II: numerical approach.
12. C. KAWADA et al. 1987 *Modern Suspension Bridge*. Tokyo: Ikou Publishing Co. (in Japanese).

APPENDIX A: MASS AND STIFFNESS MATRIX OF SUSPENSION BRIDGE ELEMENT

Consistent-mass matrix, the element gravity-stiffness matrix of the cable and the element elastic-stiffness matrix of the stiffening girder are as follows:

$$\mathbf{M}_e = \begin{bmatrix} c_1 & c_2 & c_3 & c_4 \\ & c_5 & -c_4 & c_6 \\ \text{symm.} & & c_1 & -c_2 \\ & & & c_5 \end{bmatrix}, \quad (\text{A1})$$

$$c_1 = \frac{ml}{T^2} \left(\frac{156}{420} + 8 \cdot 40S_e + 4 \cdot 8S_e^2 \right) + \frac{1 \cdot 2\rho_g I_g}{T^2 l},$$

$$c_2 = \frac{ml^2}{T^2} \left(\frac{22}{420} + 1 \cdot 1S_e + 6S_e^2 \right) + \frac{\rho_g I_g}{T^2} (0 \cdot 1 - 6S_e),$$

$$c_3 = \frac{ml}{T^2} \left(\frac{54}{420} + 3 \cdot 6S_e + 24S_e^2 \right) - \frac{1 \cdot 2\rho_g I_g}{T^2 l},$$

$$c_4 = \frac{ml^2}{T^2} \left(\frac{13}{420} + 0 \cdot 9S_e + 6S_e^2 \right) + \frac{\rho_g I_g}{T^2} (0 \cdot 1 - 6S_e), \quad (\text{A2})$$

$$c_5 = \frac{ml^3}{T^2} \left(\frac{4}{420} + 0 \cdot 2S_e + 1 \cdot 2S_e^2 \right) + \frac{\rho_g I_g l}{T^2} \left(\frac{56}{420} + 2S_e + 48S_e^2 \right),$$

$$c_6 = -\frac{ml^3}{T^2} \left(\frac{3}{420} + 0 \cdot 2S_e + 1 \cdot 2S_e^2 \right) - \frac{\rho_g I_g l}{T^2} \left(\frac{14}{420} + 2S_e - 24S_e^2 \right),$$

$$T = 1 + 12S_e,$$

$$\mathbf{K}_{eg}^e = \begin{bmatrix} a_1 & a_2 & a_1 & a_2 \\ & a_3 & -a_2 & a_4 \\ \text{symm.} & & a_1 & -a_2 \\ & & & a_3 \end{bmatrix}, \quad (\text{A3})$$

$$a_1 = (1 \cdot 2 + 24S_e + 144S_e^2)H_w/(T^2 l),$$

$$a_2 = 0 \cdot 1H_w l/(T^2 l), \quad (\text{A4})$$

$$a_3 = \left(\frac{1}{7 \cdot 5} + 2S_e + 12S_e^2 \right)H_w l^2/(T^2 l),$$

$$a_4 = -\left(\frac{1}{30} + 2S_e + 12S_e^2 \right)H_w l^2/(T^2 l),$$

$$\mathbf{K}_{eg}^e = \begin{bmatrix} b_1 & b_2 & -b_1 & b_2 \\ & b_3 & -b_2 & b_4 \\ \text{symm.} & & b_1 & -b_2 \\ & & & b_3 \end{bmatrix}, \quad (\text{A5})$$

$$\begin{aligned}
 b_1 &= 12E_g I_g / (Tl^3), & b_2 &= 6E_g I_g / (Tl^2) \\
 b_3 &= 4(1 + 3S_e)E_g I_g / (Tl), & b_4 &= 2(1 - 6S_e)E_g I_g / (Tl).
 \end{aligned}
 \tag{A6}$$

APPENDIX B: NOMENCLATURE

A	cross-sectional area
A_g	sum of the cross-sectional area of top and bottom chords (truss)
E	modulus of elasticity
f	cable sag
f_s	shear coefficient
G	shear modulus
H_w	initial horizontal component of cable tension
$H(t)$	additional horizontal component of cable tension
I_g	moment of inertia (equivalent beam) or moment of inertia of top and bottom chord about its neutral axis (truss)
\mathbf{K}_{CG}	global gravity-stiffness matrix of the cable
\mathbf{K}_{CE}	global elastic-stiffness matrix of the cable
\mathbf{K}_{EG}	global stiffness matrix of the stiffening girder
L_E	virtual length of the cable
\mathbf{M}	global consistent-mass matrix
m	mass of the bridge per unit length
u	longitudinal displacement
\mathbf{U}	global nodal displacement
v	translational displacement
\mathbf{V}_e	nodal displacement vector
β	rotational displacement
ρ	mass density
ϕ	mode shape
ω	natural frequency
<i>Subscripts</i>	
g	stiffening girder
c	cable